EXPERIMENTAL STUDY WITH DIFFERENT STRATEGIES AND AIR-DILUTION USING OPTICAL SI ENGINE FUELED WITH HYDRATED ETHANOL

M. F. Silva,
P. T. Lacava,
A. Penaranda,
M. E. Sbampato,
and L. R. Santos

Techonogical Institute of Aeronautics
Laboratório de Combustão, propulsão e energia
Bairro Vila das Acacias
São José dos Campos, São Paulo, Brasil
mayconfsilva@yahoo.com.br
placava@ita.br
amendoza@ita.br
esthersbam@gmail.com
leila@ita.br

Received: July 01, 2022
Revised: July 03, 2022
Accepted: July 14, 2022

ABSTRACT

Several dilution conditions techniques are used in internal combustion engines to increase fuel economy and reduce pollutant emissions, primarily nitrogen oxide (NOX), which are generated by the thermal pathway. Among the techniques, we can highlight air dilution (lean combustion) and exhaust gas recirculation (EGR). The control of these operations using different types of fuels and biofuels and their peculiarities, are of fundamental importance to remove the maximum efficiency from the process, generating the lowest level of emission and respecting the current legislation. Although several studies have achieved interesting results for reducing emissions and knocks thanks to the dilution of the air, it has been observed that the diluent without oxygen is more efficient. Although air dilution has a slightly lesser effect than EGR, this mode of operation can help to understand the dynamics of engine load dilution, mainly due to the complexity of EGR tests on research engines. Therefore, as a background, tests were carried out experimentally with air dilution in order to understand the behavior for the prediction of future tests with EGR. The tests were performed with hydrated ethanol and speeds of 1500 rpm and 2500 rpm. It was possible to observe that with increasing dilution, there is a gradual increase in the variability of the burn and its displacement to the region close to the inlet valve. It was observed that the dilution provided a decrease in the formation of NOX and CO and an increase in hydrocarbon emissions. Increased rotation due to increased turbulence causes changes in emission values.

Keywords: combustion, SI engine, ethanol, lean combustion, optical engine

INTRODUCTION

In order to increase fuel economy and reduce pollutant emissions, especially nitrogen oxides (NO_X), several dilution techniques are used in internal combustion engines (Heywood, 1988). Among the techniques, we can highlight the air dilution (lean combustion), used in almost all sectors of combustion technology and the technique of exhaust gas recirculation (EGR). The wide range of applications of the techniques, mainly lean combustion, seeks to take advantage of the fact that combustion processes operating under low fuel consumption conditions can have lower emissions and greater efficiency. Pollutant emissions are reduced because the flame temperature is normally low, reducing the formation of thermal nitric oxide. In addition, depletion can provide complete burning of hydrocarbons and provide complete burning of fuel, reducing HCs and CO emissions. Unfortunately, achieving these improvements and meeting the demands of practical combustion systems is complicated by low reaction rates, extinction, instabilities, moderate heat release, and sensitivity to mixing.

Exhaust gas recirculation (EGR) has the fundamental objective of recirculating a certain amount of exhaust gases, leading them to the intake manifold, mixing them with pure air. The technique, commonly applied in internal combustion engines, minimizes the accumulation of nitrogen oxides resulting from the thermal pathway.

Lack of control over the auto-ignition mechanism and heat release rate is one of the biggest challenges in implementing these models in commercial internal combustion engines. Therefore, to obtain safe, efficient, and marketable engines, it is important to have better knowledge of the various phenomena in low temperature conditions and the condition of burning in the presence of inert gases in the chamber.

The control of these operations with different types of fuels and biofuels and their peculiarities are of fundamental importance to extract maximum efficiency from the process, generating the lowest level of emission and respecting current legislation.

Because of its attractive characteristics, including octane values and spark ignition (SI) operating power without any significant changes to the engine or fuel system, ethanol has proven to be an efficient biofuel, boosting combustion, whether as a partial fuel or main. With greater vaporization heat than gasoline, the presence of ethanol in combustion

reduces the temperature of the charge and cylinder walls, ensuring lower temperature burning and helping to reduce the formation of pollutants (Heywood, 1988; Desantes et. al., 2015; Augoye et. al., 2015; Di Iorio et. al., 2015; Assad et. al., 2011). According to Varde et al. (2009), even with partial applications, experiments showed that the addition of ethanol to gasoline generated lower levels of NO_X emissions than pure gasoline.

Although several studies have achieved interesting results for the reduction of emissions and knocks with the use of air dilution, it was observed that the thinner without oxygen in its composition is more efficient. Thus, it is highlighted that the combustion gases used in the EGR recirculation is presented as a more efficient technique. Although air dilution has a slightly smaller effect than flared gas recirculation, this mode of operation can help to understand the dynamics of engine load dilution, mainly due to the complexity of EGR tests on search engines.

Therefore, tests were carried out in a spark ignition (SI) research engine with optical access with 5% hydrated ethanol in order to analyze the thermodynamic and emission effects that the dilutions act under the same conditions. In addition, the results will aid in determining the expected dilution flow for each rotation before instability.

EXPERIMENTAL PROCEDURE

To perform the tests, an AVL 5406 spark-ignition internal combustion engine with optical access, active AC dynamometer, acquisition system, and control unit was used. From its specifications, the AVL 5406 4-valve engine (2 intakes and 2 exhausts), total volume of 530 cm^3, crankshaft 144 mm, engine stroke 90 mm and piston diameter 82 mm.

The quartz combustion chamber and the 72 mm diameter fused silica window attached to the piston crown allow optical access to the interior. With the aid of an appropriate mirror inclined at 45° fixed to the bottom of the elongated piston and the radiation produced by combustion within the chamber, images can be recorded by the acquisition system. The system configuration allows access to 64mm in diameter. The experimental apparatus and the image acquisition scheme used are shown in Fig. 1.

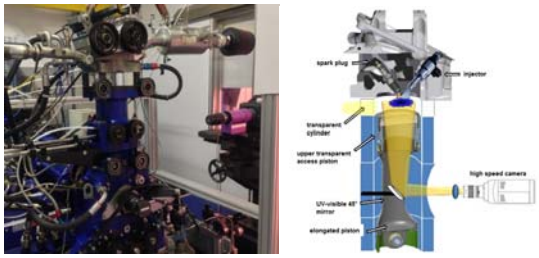

Figure 1. Experimental apparatus with AVL 5406 motor and high-speed camera and scheme of the experimental apparatus (Adapted from Catapano, et al. 2013).

A high-speed PCO.Dimax S1 camera coupled with a VS4-1845HS Scope dual intensifier and 105 f/4.5 UV-Nikon lenses was used to obtain optical data. A region of interest of 864x896 pixels was selected, a frame rate of 4500 fps for a speed of 1500 rpm, corresponding to 1 image for every 2 crank angles (CA) and a frame rate of 5000 fps for a speed of 2500 rpm, corresponding to 1 image for every 3 crank angles (CA).

The optical configuration allowed to detection of image sequences with a resolution of 91 μm/pixel. For a more complete investigation of the combustion cycles, the tests consisted of the acquisition of 62 frames per cycle. Figure 2 shows the view taken by the high-speed camera from the top of the cylinder. Possible positions for the DI injector (lateral or central) are shown in Fig. 2. The spark plug is located 5 mm above the geometric center of the chamber.

The tests were performed with central direct injection, using 5% hydrated ethanol fuel (E95W5), the injection pressure of 100 bar, and spark ignition at -14 CA ATDC. Tests were performed with engine speed of 1500 rpm and 2500 rpm with IMEP 3.0 and 1.8, respectively. Such engine speeds, in addition to providing greater sensitivity in controlling the pressure in the intake manifold, help to compare the turbulence behavior inside the engine. The experiments were carried out with constant fuel flow and variable load for air dilution until operation became unstable (Cov% IMEP> 5%). For each engine speed, a fixed spark advance was selected, where the criterion was an intermediate value between the MBT (Maximum Brake Torque) for the stoichiometric and lean conditions.

The load definition, determined by the IMEP, was selected by the simulation of a gear shift condition where the product of the load and speed of 1500rpm is the same as the product of the load and speed of 2500 rpm. However, it was necessary the execution of several tests reproduce the loads for different lean mixtures with the same load.

After these tests, the experimental conditions of engine speed at 1500 rpm, IMEP 3.0 bar and engine speed of 2500 rpm with IMEP 1.8 bar were defined. Air-fuel ratio data of lambda 1.0 (baseline), λ 1.2, 1.4 and 1.5 (unstable condition) for 1500 rpm were obtained. For 2500 rpm, λ 1.0, 1.2, 1.3 and 1.4 were obtained (unstable condition).

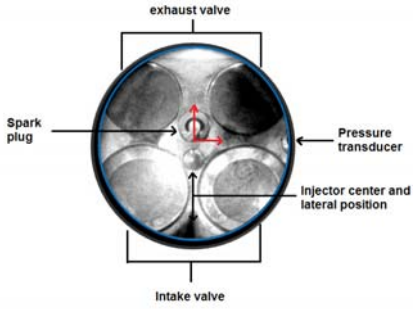

Figure 2. Combustion chamber geometry, with intake and exhaust valves, spark plug and pressure transducer.

The combustion products species concentrations were measured in the exhaust gas stream using a Multigas 2030 spectrometer analyzer (MKS Instruments).

The MKS 2030 spectrometer works based on Fourier Transform Infrared (FTIR) principle and can acquire multiple gas species at same time. The detection limit is 1 ppm for CO and 0.5 ppm for formaldehyde, NO, NO_2, and ethanol; the equipment accuracy is 5% for all the chemical species. Emission data were adjusted for dry basis and corrected to 3% oxygen for a pattern of oxygen consumption in the relation of the oxygen presented in pure air (considered here 20.9%).

RESULTS

To study the behavior and operating conditions of the internal combustion engine, images were acquired through the bottom view of the combustion chamber. This visualization allows a better analysis and in obtaining information about flame propagation. Figures 4-6 show the flame propagation images for combustion at the speed of 1500 rpm, for λ 1.0, 1.2 and 1.4, respectively, from spark ignition.

From this, it is observed that variability and a decentralization of the flame is provided as the increase in air dilution occurs. In addition to a lower definition of the flame edge, greater variability of its circularity, a lower propagation speed is observed with the increase of air dilution. Some of the possible reasons for the displacement of the flame with the increase in dilution could be the more intense tumble movement characteristic of this engine and the greater amount of fuel in the region of the intake valve (Abrantes, 2017).

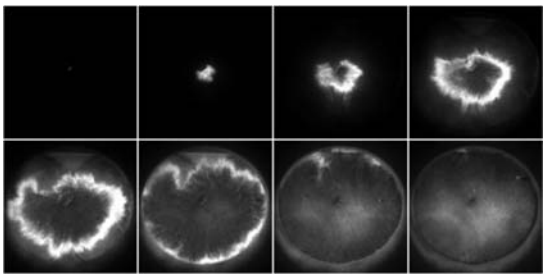

Figure 3. The sequence of images from the bottom view of the flame propagation from spark ignition for 1500 rpm and air-fuel ratio λ = 1.0.

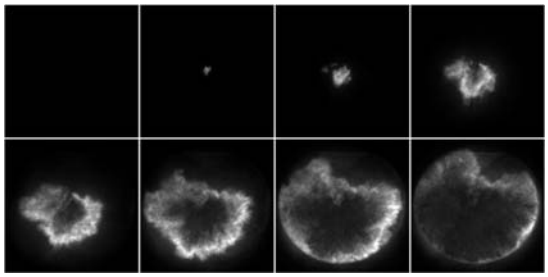

Figure 4. The sequence of images from the bottom view of the flame propagation from spark ignition for 1500 rpm and air-fuel ratio λ = 1.2.

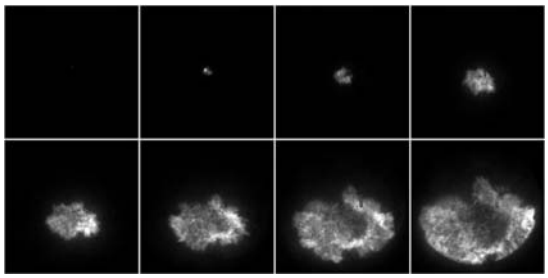

Figure 5. The sequence of images from the bottom view of the flame propagation from spark ignition for 1500 rpm and air-fuel ratio λ = 1.4.

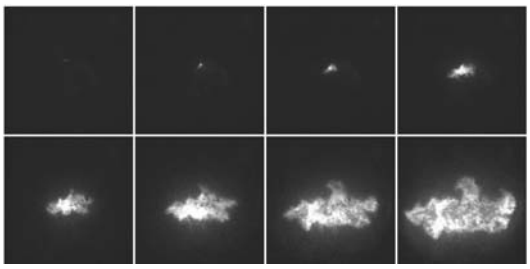

Figure 6. The sequence of images from the bottom view of the flame propagation from spark ignition for 1500 rpm and air-fuel ratio λ = 1.4.

Table 1 to Table 4 show the IMEP, maximum cylinder pressure, AI50% and lambda values for a burn condition for an average of the last 100 engine cycles in operation for the 1500 rpm experiments and lambda values of 1.0, 1.2, 1.4 and 1.5.

In these figures, it is possible to observe that the IMEP coefficient of variability (COV) is proportional to the increase in the lambda value, with a higher value of COVImep = 16.32% for a lambda of 1.5 (Table 4). It is also possible to notice that the average behavior of the IMEP presents several instabilities during the 100 measured cycles.

Table 1. Experimental results for the test at 1500 rpm and lambda 1.0. Top image: lambda and IMEP behavior during the last 100 cycles; bottom image:

summary of the average indicating results of the last 100 cycles.

	IMEP [bar]	PMAX [bar]	AI10% [deg]	AI50% [deg]	Lambda -
Min	2.98	15.81	1.00	9.00	1.01
Mean	3.04	17.50	3.05	12.61	1.03
Max	3.16	19.20	4.75	16.50	1.05
Std	0.040	0.738	0.958	1.60	0.009
Cov%	1.30	4.22	31.42	12.67	0.833

Speed [rpm]	P Intake [mbar]	Throttle %	IGN [ºCA]
1500	-417	7.6	-14
SOI [ºCA]	DOI [ms]	mAir [kg/h]	P Rail [bar]
-290	3.32	10.65	100

Table 2. Experimental results for the test at 1500 rpm and lambda 1.2. Top image: lambda and IMEP behavior during the last 100 cycles; bottom image: summary of the average indicating results of the last 100 cycles.

	IMEP [bar]	PMAX [bar]	AI10% [deg]	AI50% [deg]	Lambda -
Min	2.95	13.39	3.00	11.75	1.20
Mean	3.05	16.15	5.60	16.23	1.23
Max	3.16	18.25	10.25	23.00	1.27
Std	0.038	1.06	1.57	2.38	0.013
Cov%	1.25	6.54	28.12	14.67	1.03

Speed [rpm]	P Intake [mbar]	Throttle %	IGN [ºCA]
1500	-366	8.2	-14
SOI [ºCA]	DOI [ms]	mAir [kg/h]	P Rail [bar]
-290	3.15	11.73	100

Table 3. Experimental results for the test at 1500 rpm and lambda 1.4. Top image: lambda and IMEP behavior during the last 100 cycles; bottom image: summary of the average indicating results of the last 100 cycles.

	IMEP [bar]	PMAX [bar]	AI10% [deg]	AI50% [deg]	Lambda -
Min	2.57	10.37	7.00	20.00	1.40
Mean	3.00	12.85	10.86	26.61	1.43
Max	3.23	15.50	16.25	36.50	1.47
Std	0.145	1.28	2.15	4.12	0.016
Cov%	4.83	9.97	19.80	15.48	1.14

Speed [rpm]	P Intake [mbar]	Throttle %	IGN [ºCA]
1500	-301	9.2	-14
SOI [ºCA]	DOI [ms]	mAir [kg/h]	P Rail [bar]
-290	3.14	13.27	100

Table 4. Experimental results for the test at 1500 rpm and lambda 1.5. Top image: lambda and IMEP behavior during the last 100 cycles; bottom image: summary of the average indicating results of the last 100 cycles.

	IMEP [bar]	PMAX [bar]	AI10% [deg]	AI50% [deg]	Lambda -
Min	1.15	10.36	10.00	24.75	1.47
Mean	2.24	10.72	16.29	37.69	1.52
Max	2.81	13.35	25.00	50.00	1.58
Std	0.365	0.537	3.12	6.07	0.027
Cov%	16.32	5.00	19.13	16.10	1.77

Speed [rpm]	P Intake [mbar]	Throttle %	IGN [ºCA]
1500	-296	9.4	-14
SOI [ºCA]	DOI [ms]	mAir [kg/h]	P Rail [bar]
-290	3.09	13.7	100

Figure 7 shows the average cylinder pressure curves for all cases of 1500 rpm. It is possible to see the influence of increased air and the influence of variability on the IMEP for cases with 1.4 and 1.5 lambda. In addition, it is seen that the dilution causes the pressure curve displacement, which can also be observed in the values of AI10% and AI50% of the previous tables and in the burnt mass fraction graphs where the flame propagation is slower when measured that dilution occurs. This behavior is also due to the fixed ignition advance.

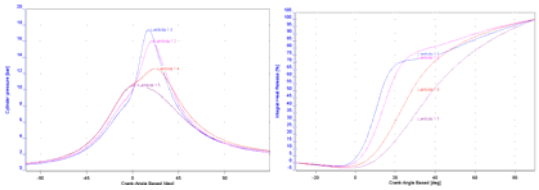

Figure 7. Average cylinder pressure curves and average integral heat release curves for 1500 rpm; IMEP 3.0 bar, for the bottom view experiments.

From Fig. 8 to Fig. 10, the average results of gas emissions for the experiments performed with 1500 rpm and IMEP 3.0 are presented.

It was observed that carbon dioxide (CO_2) presented a slight decrease with increasing dilution in air, however, its value remained close. As for carbon monoxide (CO) and NO_X emissions, a large decrease was provided as dilution by air occurred. There is a significant decrease for NO_X (about 10 times less between $\lambda = 1$ and $\lambda = 1.43$). With the increase in the amount of air present in the combustion chamber, the decrease in temperature caused by this leads to less formation of thermal NOx, due to the lower burning temperature.

It is also observed that formaldehyde and THC-ethanol emissions increased slightly from $\lambda = 1$ to $\lambda = 1.25$ and decreased between $\lambda = 1.25$ and $\lambda = 1.43$. Emissions from unburned ethanol have been steadily increasing with increasing dilution.

In lean combustion, excess air can act in addition to reducing the flame temperature, but also limiting the ability of the reactions to reach equilibrium, which can lead to an increase in exhaust hydrocarbons. Furthermore, cooling the combustion chamber wall can contribute to cooling (Dunn-Rankin et. al., 2016 and Turns, 2013).

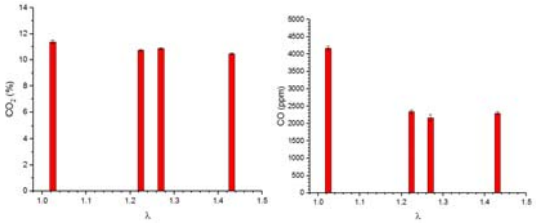

Figure 8. Emissions gas measurement of CO_2 and CO, 1500 rpm, IMEP 3.0 bar.

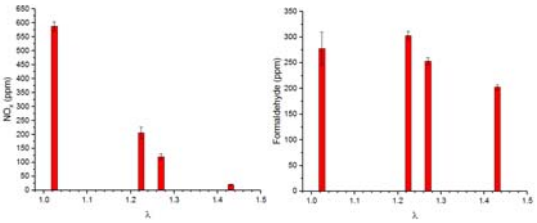

Figure 9. Emissions gas measurement of NOx and formaldehyde, 1500 rpm, IMEP 3.0 bar.

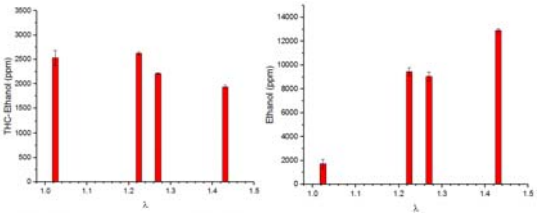

Figure 10. Emissions gas measurement of THC-ethanol and unburned ethanol, 1500 rpm, IMEP 3.0 bar.

Similar to the 1500 rpm data, the images were also acquired from the bottom view, obtaining the combustion flame propagation for the same air-fuel ratios for 2500 rpm in Fig. 11 to Fig. 13.

With the same behavior as the 1500 rpm images, the 2500 rpm images show an increase in the variability, distortion and displacement of the flame with the increase in air dilution. Furthermore, the lowest propagation speed is also observed.

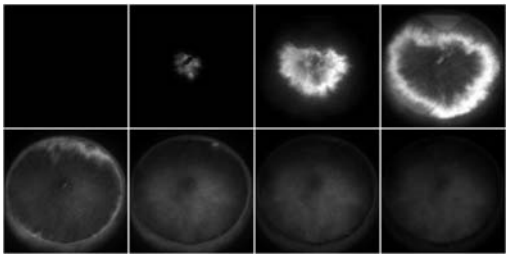

Figure 11. The sequence of images from the bottom view of the flame propagation from spark ignition for 2500 rpm and air-fuel ratio λ = 1.0.

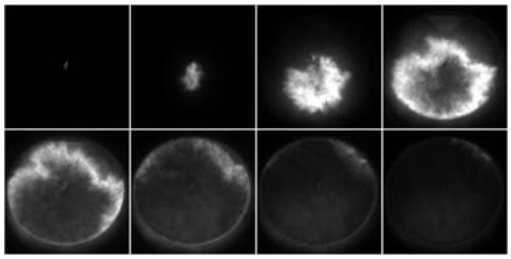

Figure 12. The sequence of images from the bottom view of the flame propagation from spark ignition for 2500 rpm and air-fuel ratio λ = 1.2.

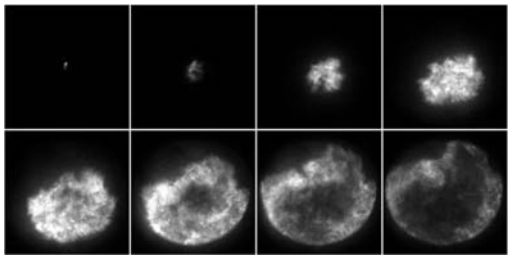

Figure 13. The sequence of images from the bottom view of the flame propagation from spark ignition for 2500 rpm and air-fuel ratio λ = 1.4.

Table 5 to Table 8 show IMEP, maximum cylinder pressure, AI50% and lambda values for an ignition condition for an average of the last 100 engine cycles in drive operation for the experiments at 2500 rpm and lambda values of 1.0, 1.2, 1.3 and 1.4, respectively.

In these figures, it is possible to observe that the conditions are similar to the 1500 rpm experiments. It was observed that the IMEP coefficient of variability (COV) is proportional to the increase in the lambda value, with a higher value of COV = 27.74% for a lambda of 1.4 (Tab. 8), it is also possible to notice that the average behavior of the IMEP presents several instabilities during the 100 measured cycles.

Table 5. Experimental results for the test at 2500 rpm and lambda 1.0. Top image: lambda and IMEP behavior during the last 100 cycles; bottom image: summary of the average indicating results of the last 100 cycles.

	IMEP [bar]	PMAX [bar]	AI10% [deg]	AI50% [deg]	Lambda -
Min	1.69	11.62	-3.50	4.00	0.993
Mean	1.79	13.08	-0.860	8.00	1.00
Max	1.87	14.23	2.00	12.50	1.01
Std	0.037	0.597	1.26	1.97	0.005
Cov%	2.06	4.56	146.5	24.67	0.464

Speed [rpm]	P Intake [mbar]	Throttle %	IGN [ºCA]

1500	-548	7.6	-20
SOI [ºCA]	DOI [ms]	mAir [kg/h]	P Rail [bar]
-290	2.15	11.21	100

Table 6. Experimental results for the test at 2500 rpm and lambda 1.2. Top image: lambda and IMEP behavior during the last 100 cycles; bottom image: summary of the average indicating results of the last 100 cycles.

	IMEP [bar]	PMAX [bar]	AI10% [deg]	AI50% [deg]	Lambda -
Min	1.69	9.98	-1.00	7.00	1.20
Mean	1.80	11.60	2.40	13.56	1.21
Max	1.89	13.63	6.25	19.50	1.22
Std	0.045	0.823	1.62	2.87	0.005
Cov%	2.48	7.09	67.72	21.15	0.426

Speed [rpm]	P Intake [mbar]	Throttle %	IGN [ºCA]
1500	-516	8.2	-20
SOI [ºCA]	DOI [ms]	mAir [kg/h]	P Rail [bar]
-290	1.97	12.48	100

Table 7. Experimental results for the test at 2500 rpm and lambda 1.3. Top image: lambda and IMEP behavior during the last 100 cycles; bottom image: summary of the average indicating results of the last 100 cycles.

	IMEP [bar]	PMAX [bar]	AI10% [deg]	AI50% [deg]	Lambda -
Min	1.66	8.18	10.00	12.50	1.30
Mean	1.83	10.49	5.22	18.75	1.32
Max	1.91	12.34	12.00	27.50	1.35
Std	0.058	1.00	2.39	3.74	0.009
Cov%	3.15	9.58	45.80	19.94	0.707

Speed [rpm]	P Intake [mbar]	Throttle %	IGN [ºCA]
1500	-489	8.5	-20
SOI [ºCA]	DOI [ms]	mAir [kg/h]	P Rail [bar]
-290	2.03	13.68	100

Table 8. Experimental results for the test at 2500 rpm and lambda 1.4. Top image: lambda and IMEP behavior during the last 100 cycles; bottom image: summary of the average indicating results of the last 100 cycles.

	IMEP [bar]	PMAX [bar]	AI10% [deg]	AI50% [deg]	Lambda -
Min	-0.613	7.14	4.00	16.00	1.40
Mean	1.32	8.10	11.50	30.52	1.44
Max	1.90	10.82	40.00	56.00	1.58
Std	0.366	0.872	5.60	7.26	0.028
Cov%	27.74	10.76	48.67	23.80	1.96

Speed [rpm]	P Intake [mbar]	Throttle %	IGN [ºCA]
1500	-477	9	-20
SOI [ºCA]	DOI [ms]	mAir [kg/h]	P Rail [bar]
-290	1.94	13.96	100

Figure 14 shows the curves of the average cylinder pressure for all cases of 2500 rpm. It is possible to see the influence of the increase in air and the influence of variability on the IMEP for the case with lambda 1.4. In addition, the influence of air dilution on the burned mass fraction during the combustion process is observed, showing that the flame propagation is slower for lean mixtures, a condition similar to the 1500 rpm cases.

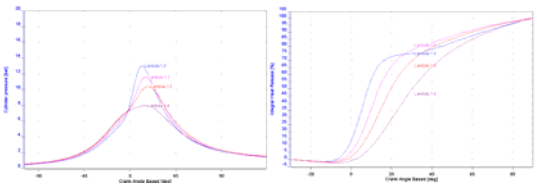

Figure 14. Average cylinder pressure curves and average integral heat release curves for 2500 rpm; IMEP 1.8 bar cases, for the bottom view experiments.

From Fig. 15 to Fig. 17, the average results of gas emissions for the experiments performed with 2500 rpm are presented. For carbon dioxide (CO_2) emissions, a slight increase was shown between $\lambda = 1$ and $\lambda = 1.21$ and a slight decrease between $\lambda = 1.24$ and $\lambda = 1.34$. However, the results are close. As for the NO_X emission, there is a decrease with dilution (about 7 times less between $\lambda = 1$ and $\lambda = 1.34$). For formaldehyde and THC-ethanol emissions increased considerably between $\lambda = 1$ and $\lambda = 1.24$ and decreased slightly between $\lambda = 1.24$ and $\lambda = 1.34$, the same behavior of the tests with 1500 rpm. The emission of unburnt ethanol was observed to increase steadily with increasing dilution.

Concerning the experiments at 1500 rpm, the variations observed at 2500 rpm differed only in the case of CO_2 and CO. In the case of 1500 rpm, there was a continuous decrease with increasing dilution.

Comparing the emission of gases between the experiments at 1500 rpm and 2500 rpm for the same dilution, it is observed that the CO emission was lower for the condition at 2500 rpm for $\lambda = 1$. For λ greater

than 1.2, the emissions at 2500 rpm were higher. When compared NO_X emissions, it is observed that it was lower for experiments at 2500 rpm. For formaldehyde emissions, as well as THC-ethanol emissions, it was about 5 smaller for 2500 rpm in the condition of $\lambda = 1$ and for the other dilutions, the difference in emissions between the two engine speeds was small. For all dilutions, the emission of unburnt ethanol was lower for the 2500 rpm experiments.

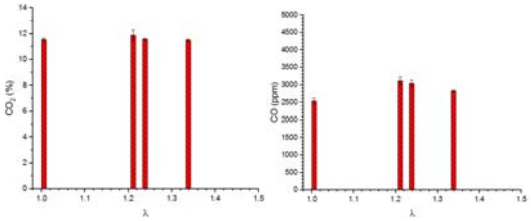

Figure 15. Emissions gas measurement of CO_2 and CO, 2500 rpm, IMEP 1.8 bar.

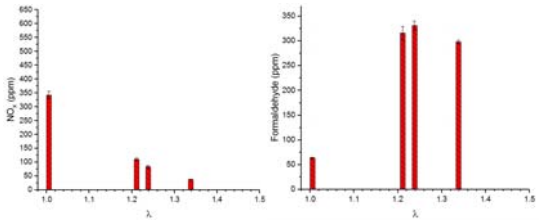

Figure 16. Emissions gas measurement of NO_X and formaldehyde, 2500 rpm, IMEP 1.8 bar.

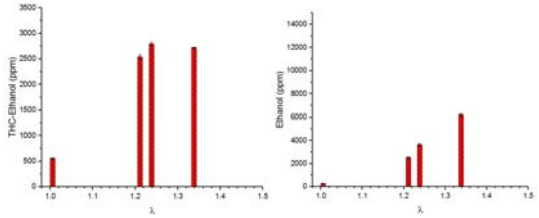

Figure 17. Emissions gas measurement of THC-ethanol and unburned ethanol, 2500 rpm, IMEP 1.8 bar.

CONCLUSION

In the present work, the behavior of air dilution in an internal combustion engine by central direct injection mode using hydrated ethanol with 5% as fuel was analyzed from optical, thermodynamic and emission data. With the increase in dilution, the images showed a gradual increase in the variability of the flame and in its displacement to the region of the inlet valve. This is due to the more characteristic tumble movement in the engine used and to the presence of a greater amount of fuel in that region.

When analyzing the thermodynamic data, it is observed that the same behavior of the images with the linear increase in variability. CovImep values demonstrate this behavior for both engine speeds. Both for 1500 rpm and for 2500 rpm, the 1.5 and 1.4 lambdas, respectively, presented very unstable results. To achieve better results, it is necessary to make modifications to the ignition advance to obtain AI50% results closer to the stoichiometric data. The tests are shown to be important as a preliminary basis to understand the behavior and subsequent comparison with the application of EGR.

ACKNOWLEDGEMENTS

This work was supported by LCPE-ITA and FAPESP-PSA.

REFERENCES

Heywood, J.B., 1988. *Internal Combustion Engine Fundamentals*. McGraw-Hill, Ed.; 1°.; McGraw-Hill: New York, USA.

Desantes, J.M., López, J.J., Molina, S., López-Pintor, D., 2015. "Design of synthetic EGR and simulation study of the effect of simplified formulations on the ignition delay of isooctane and n-heptane". *Energy Convers. Manag*, *96*, 521–531, doi:10.1016/j.enconman.2015.03.003.

Augoye, A., Aleiferis, P., 2015. "Characterization of Flame Development with Hydrous and Anhydrous Ethanol Fuels in a Spark-Ignition Engine with Direct Injection and Port Injection Systems". *SAE Tech. Pap*, *01*, doi:10.4271/2014-01-2623.

Di Iorio, S., Sementa, P., Vaglieco, B., 2015. "Experimental Characterization of an Ethanol DI - Gasoline PFI and Gasoline DI - Gasoline PFI Dual Fuel Small Displacement SI Engine". *SAE Tech. Pap.*, 1–8, doi:https://doi.org/10.4271/2015-01-0848.

Assad, M.S., Kucharchuk, I.G., Penyazkov, O.G., Rusetskii, A.M., Chornyi, A.D., 2011. "Influence of Ethanol on the Operating Parameters of an Internal-Combustion Engine". *J. Eng. Phys. Thermophys*, *84*, 1219–1224.

Varde, K.S.; Manoharan, N.K., 2009. "Characterization of exhaust emissions in a SI engine using E85 and cooled EGR". *SAE Tech. Pap*, *4970*, doi:10.4271/2009-01-1952.

Catapano, F., Sementa, P., Vaglieco, B.M., 2013. "Optical characterization of bio-ethanol injection and combustion in a small DISI engine for two wheels vehicles". *Fuel*, *106*, 651–666, doi:10.1016/j.fuel.2012.11.064.

Abrates, T. T. da S. *Aplicação da técnica PIV em um motor de combustão interna com acesso óptico para estudo dos fenômenos Tumble e Swirl*. [s.l.] Instituto Tecnológico de Aeronáutica, 2017.

Dunn-Rankin, D., Therkelsen, P., 2016. "Lean Combustion Technology and Control". Elsevier, London, UK.

Turns, Stephen R., 2013."Introdução à combustão: Conceitos eaplicações". McGrall Hill AMGH, 3. ed.